

The Cosmic Evolution of Metallicity from the SDSS Fossil Record

Benjamin Panter¹, Raul Jimenez², Alan F. Heavens¹, Stephane Charlot³

¹*Institute for Astronomy, SUPA, University of Edinburgh, Royal Observatory, Edinburgh EH9-3HJ, UK; bdp, afh@roe.ac.uk*

²*Institute of Space Sciences(ICE), CSIC-IEEC/ICREA, UAB campus, Barcelona, Spain; jimenez@ieec.uab.es*

³*Institut d'Astrophysique de Paris, UMR 7095, 98 bis Boulevard Arago, F-75014 Paris, France; charlot@iap.fr*

24 October 2018

ABSTRACT

We present the time evolution of the stellar metallicity for SDSS galaxies, a sample that spans five orders of magnitude in stellar mass ($10^7 - 10^{12} M_{\odot}$). Assuming the Bruzual & Charlot (2003) stellar population models, we find that more massive galaxies are more metal-rich than less massive ones at all redshifts; the mass-metallicity relation is imprinted in galaxies from the epoch of formation. For galaxies with present stellar masses $> 10^{10} M_{\odot}$, the time evolution of stellar metallicity is very weak, with at most 0.2 – 0.3 dex over a Hubble time- for this reason the mass-metallicity relation evolves little with redshift. However, for galaxies with present stellar masses $< 10^{10} M_{\odot}$, the evolution is significant, with metallicity increasing by more than a decade from redshift 3 to the present. By being able to recover the metallicity history, we have managed to identify the origin of a recent discrepancy between the metallicity recovered from nebular lines and absorption lines. As expected, we show that the young population dominates the former while the old population the latter. We have investigated the dependence on the stellar models used and find that older stellar population synthesis codes do not produce a clear result. Finally, we have explored the relationship between cluster environment and metallicity, and find a strong correlation in the sense that galaxies in high density regions have high metallicity.

Key words: galaxies: evolution, galaxies: statistics, galaxies: abundances

1 INTRODUCTION

The quality of spectra of the observed light of unresolved stellar populations has reached a sufficient accuracy that it is now possible to make detailed studies of the physical properties of the stellar populations in these galaxies. While much attention has focussed on the time evolution of the star formation rate of galaxies (Panter et al. 2003; Heavens et al. 2004; Panter et al. 2004; Cid Fernandes et al. 2005; Mathis et al. 2006; Ocvirk et al. 2006), a closely related quantity, the evolution of the metallicity of the star forming gas in galaxies, has not received as much attention (Panter et al. 2003; Erb et al. 2006; Bouché et al. 2007; Cid Fernandes et al. 2007; Erb 2008; Gallazzi et al. 2008). One reason is that while it is relatively straightforward to measure the star formation rate from massive stars at different redshifts, it is not easy to determine its metallicity, which requires high-quality spectra. Further, in order to cover a large range in mass and lookback time one would need to observe a very large area of the sky, of the order of thousands of square degrees.

One alternative approach is to use the fossil record in the local universe and reconstruct the star and metallicity

history from this record. This however has its own limitations (Ocvirk et al. 2006; Panter et al. 2007; Tojeiro et al. 2007). Using MOPED, a tool that allows rapid extraction of the physical parameters of the stellar populations of galaxies from their spectra, our group has shown how it is possible to use the fossil record to obtain information about the stellar populations of galaxies at large lookback times (Panter et al. 2007). In this work we concentrate on what can be learned about the metallicity of those stellar populations.

The evolution of metallicity of the stellar populations of galaxies as a function of redshift is highly relevant as it can tell us about how the interstellar medium is being enriched, potentially what the initial mass function is (provided the theoretical yields of stars are well known) and how this enrichment depends on environment (Sheth et al. 2006) or mass, star formation history and age of the galaxy (Panter et al. 2007).

Determining the metallicity history of galaxies has indeed a long history. The first attempt is to use our own galaxy as representative and measure metallicities in its individual stars or stellar clusters (see, for example, the review by Freeman & Bland-Hawthorn (2002)). There are two ma-

major advantages: one can obtain high S/N detailed spectra, and the stellar populations are individually resolved. The main disadvantage is that our galaxy is not typical of others in the Universe.

The second route is to determine the metallicity of galaxies from the spectrum of their integrated light. The pioneering grid of models by Worthey (1994) allowed this for simple stellar populations, i.e. elliptical galaxies. His models provided Lick equivalent widths in the optical region that were sensitive to the overall metallicity of the stellar population. Indeed the application of this technique has allowed many researchers to determine the metallicity of galaxies in the nearby (e.g. Gallazzi et al. (2006)) and distant (e.g. Pettini (2001)) universe. The ratios of various emission lines can also be used to determine the metallicity of the gas in a galaxy, although careful calibration is required (Kewley & Dopita 2002; Tremonti et al. 2004; Erb et al. 2006).

However, Heavens et al. (2004) have shown that for an ensemble of galaxies it is possible to go beyond simply recovering the mass-weighted metallicity of the stars and recover the metallicity history in many time bins. This is not necessarily true for individual galaxies (e.g. Ocvirk et al. (2006); Tojeiro et al. (2007)), which may have noisy recoveries, but has been shown to be unbiased when averaged over a sufficiently large sample. The recovery of the star formation history and metallicity for galaxies is similar to the “population boxes” for nearby resolved stellar populations in local group galaxies (e.g. Gallart et al. (2005)).

In this paper we recover the metallicity history of SDSS galaxies from their spectra. We determine its evolution as a function of mass, how the mass-metallicity relation depends on the age of the stellar population and how sensitive our findings are to the stellar population models used. The paper is organized as follows: in §2 we describe the SDSS sample used and in §3 we describe briefly the method to determine metallicities. In §4 we show the derived cosmic metallicity history and in §5 we present a map of the stellar metallicity history. §6 and 7 concern the mass-metallicity relation and how it evolves with redshift and mass. §8 shows the impact of the choice of stellar population model on our findings. We conclude with a general discussion of our findings in §9.

2 THE SAMPLE

As described in Panter et al. (2007), the MOPED algorithm has been used to extract star formation and metallicity histories of a magnitude limited sample of about 300,000 galaxies drawn from the Third Data Release of the Sloan Digital Sky Survey (SDSS DR3; Abazajian et al. (2005)).

Our main galaxy sample is determined by red apparent magnitude limits of $15.0 \leq m_r \leq 17.77$, and we also place a cut on surface brightness of $\mu_r < 23.0$. The magnitude limits are set by the SDSS target selection criteria, as discussed in Abazajian et al. (2005). The target criteria for surface brightness was $\mu_r < 24.5$, although for $\mu_r > 23.0$ galaxies are included only in certain atmospheric conditions. In order to remove any bias we have therefore cut our sample at $\mu_r < 23.0$. At low redshifts the Sloan galaxies are subject to shredding - where a nearby large galaxy is split by the target selection algorithm into several smaller sources. To reduce

this effect, for our star formation analysis we use a range of $0.005 < z < 0.34$. We want to derive properties that avoid dependence on the SFH of the galaxies, and hence wish to avoid inverse V_{max} weighting where possible. We therefore choose mass cuts around a narrow redshift range of 0.1 for the deriving the cosmic metallicity evolution, and show colors normalised to the total number of galaxies in that mass range in the mass-metallicity diagrams.

3 DETERMINING THE METALLICITIES OF GALAXIES

In order to determine the optimal multi-population fit for each spectrum it is necessary to allow as free a star formation history as possible. A parametrization of 11 SSPs spaced logarithmically in lookback time, each with independent and variable metallicity, was allowed along with a one parameter slab extinction based on the Gordon et al. (2003) LMC curve. In order to fully assess the resulting 23 dimensional likelihood surface it was necessary to use the MOPED¹ (Heavens et al. 2000; Reichardt et al. 2001) algorithm coupled with a Markov Chain Monte Carlo search method (Panter et al. 2003), developed to use high spectral resolution models (Panter et al. 2007). For each galaxy the best solutions from a series of 100 randomly-seeded conjugate gradient searches were used to seed a Markov chain of 10^6 steps. The individual search traces were examined to confirm adequate exploration of the parameter space and estimate solution convergence.

In our approach, for each galaxy we describe its star formation by 11 lookback time bins (spaced logarithmically) and for each of these we determine the mass fraction transformed into stars and its metallicity. The first interesting result, before looking at the metallicity history of galaxies, is to look at the overall metallicity of the stars in SDSS galaxies today. It is important to realize that there must be some weighting of the metallicity values recovered - the metallicity of a population that contributes very little light to the final spectrum is not constrained, so should be discounted. Since the MOPED method recovers the complete star formation history of a galaxy it is possible to calculate the average metallicity with different weights. Traditional Lick index analysis considers the light-weighted metallicity, but with knowledge of the SFH and IMF it is possible to determine present mass fraction (PMF) or original star formation fraction (SFF)² average metallicities weighted by either.

In Fig. 1 we illustrate how a synthetic galaxy spectrum responds to changes in metallicity history, by comparing a synthetic spectrum created using the mean star and metallicity history of SDSS galaxies recovered by MOPED with models that have the same star formation history but different metallicity histories. It is clear that changing the metallicity has a significant effect on both the continuum level and depth of absorption features.

We can distinguish regions in wavelength that are driving the differences coinciding with H, Ca, Fe and Mg absorption lines. The continuum shape blueward of 4000Å also has

¹ Massively Optimized Parameter Estimation and Data Compression

² i.e., the fraction of total star formation over the galaxy’s history

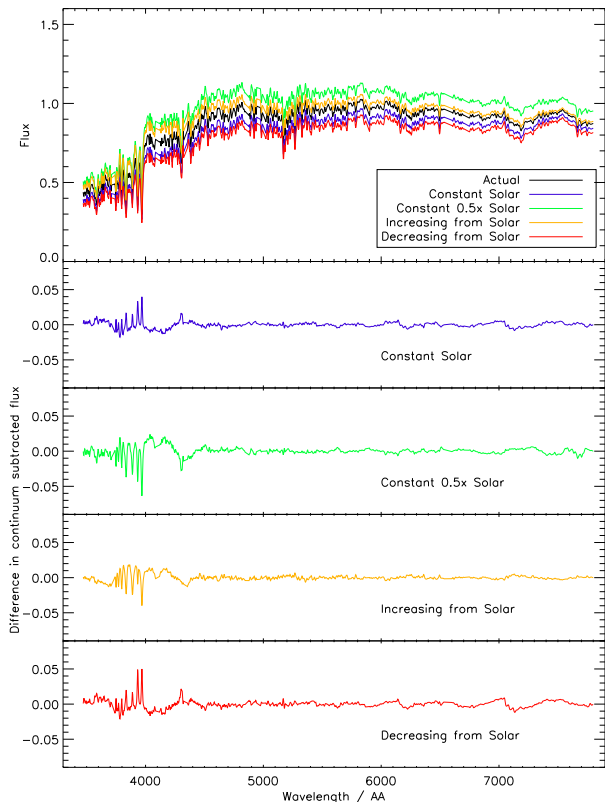


Figure 1. A synthetic spectrum corresponding to the mean star formation history of SDSS galaxies, and the effect of changing the metallicity history while maintaining the same star formation history. The lower panels show the difference between the continuum-subtracted mean spectrum and a model produced using the different continuum-subtracted alternate metallicity models, illustrating that changes in metallicity history can be seen in both the low and high frequency spectral signal. In this figure, increasing from solar refers to an initial metallicity of Z_{\odot} in the oldest bin rising to $2.5Z_{\odot}$ in the youngest and decreasing from solar an initial metallicity of Z_{\odot} falling to $0.02Z_{\odot}$.

an impact, but in this plot we are showing only the high frequency signal of the residuals normalized to the continuum. While traditional indices based approaches will consider some subset of this data, by analyzing the full spectrum we are able to determine the metallicity of individual galaxies more accurately.

4 THE COSMIC METALLICITY HISTORY

In order to combine the metallicity histories of many galaxies at different redshifts it is necessary to estimate metallicity histories in a common time frame. In previous work we have formed complex transform functions to redistribute a galaxies SF in a new set of bins, but in this case we instead chose a narrow redshift range of galaxies ($|z-0.1| < 0.01$). For our common bins we use the original time bins (see Panter et al. (2007)) with $t = 0$ at $z = 0.1$. This gives a sample of 42160 galaxies.

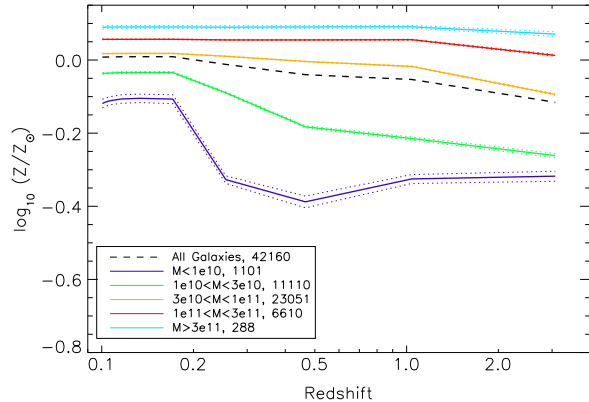


Figure 2. Bulk metallicity of stars in SDSS galaxies for different stellar masses. This is the average metallicity of all stars present at a particular redshift, regardless of age. To avoid possible errors from shifting bins we have chosen a narrow redshift range centred at $z = 0.1$. The number of galaxies in each mass range is given in the inset. Note that more massive galaxies are more metal rich than less massive galaxies. The enrichment is very flat as a function of redshift for the more massive galaxies, as the bulk of their stars formed early and the tiny amount of recent SF has not been sufficient to change the bulk metallicity. The dotted lines correspond to a 1σ bootstrap error.

The simplest interpretation of the metallicity history is that of the bulk of stars in a galaxy at a given time. To calculate this for each bin we weight the metallicity in the bins up to that point by the mass of stars remaining from that bin (ie, we include recycling). This traces the average metallicity of stars in a galaxy over its evolution, and is shown in Fig. 2.

The individual metallicity histories of each galaxy can also be combined to give the mass-weighted cosmic metallicity history of the star forming gas. To calculate this we average the metallicities for a given bin, weighted by the mass of that population. We must also impose a cut to ensure that the metallicity of populations which have a very small contribution to the spectrum are not considered, as these have poorly determined metallicity and give results dependent on the metallicity prior. To avoid this contamination we add a further cut: to contribute to the average of a particular time bin a galaxy must have $> 25\%$ of its spectral flux in that bin (see Fig. 3).

Weighting by bin mass obviously biases the results towards high-mass galaxies. We also present results using a weighting scheme that uses the fraction of the total spectral flux. Weighting by mass means that there is a slight bias towards older populations, which may not be as well determined as for a given mass as the younger populations give much more light. To calculate the cosmic metallicity history the metallicities in the bins are then averaged, weighted by the fractional contribution of the bin to the galaxy luminosity. In this weighting scheme a galaxy's mass is irrelevant. The corresponding cosmic metallicity history is shown in Fig. 4 and is very similar to the flux-weighted history (Fig. 3).

The first thing we learn is that most metals are locked in the most massive galaxies and that the metallicity evo-

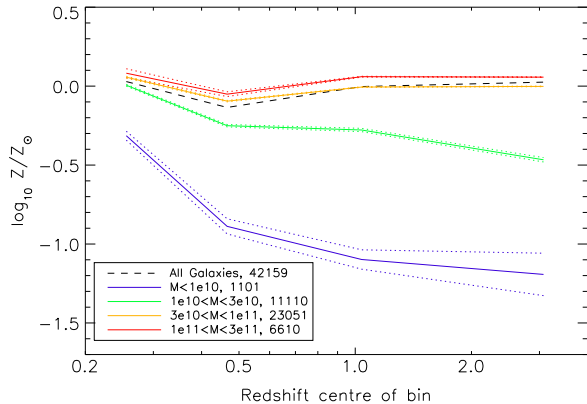


Figure 3. Average metallicity for different stellar masses, as in Fig. 1 except for star forming gas rather than stars.

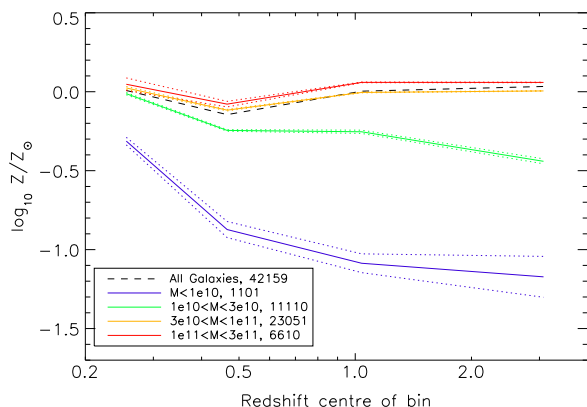


Figure 4. Same as Fig. 3 but for a total fractional spectral flux weighted average.

lution for each mass range is relatively flat as a function of redshift, with variations of 0.1-0.2 dex for each mass range. Note that a similar trend is found for a light-weighted plot. Our results compare favourably with the trends observed at high redshift by Maiolino et al. (2007). If we look at their Fig. 3 and compare their abundance as a function of redshift for a stellar mass of $1 \times 10^{10} M_{\odot}$ with our green line in Fig. 1, 2 and 3 we find that their abundance values at $z = 3, 0.07$ and 0 are $\log(Z/Z_{\odot}) = -0.54, -0.1, 0.1$ respectively, assuming that $12 + \log(O/H)_{\odot} = 8.66$. This compares with our derived values, for the same redshift intervals, of $-0.5, -0.2, 0.0$, which is within 0.1 dex of their values, which is remarkable. Any conclusions are subject to model choice, as we explore in §8.

5 MAPPING THE METALLICITY EVOLUTION OF THE UNIVERSE

The SDSS-DR3 spectroscopic footprint covers 3732 sq. deg., roughly 10% of the sky. We use the metallicity history of the galaxies to create maps over this area of the enrichment his-

Table 1. Pearson correlations of metallicity and number of cluster galaxies in a cell

z	Smoothing Radius($^{\circ}$)			
	0	2	3	4
0.187	0.091	0.118	0.104	0.079
0.456	0.101	0.167	0.171	0.171
1.21	0.131	0.213	0.212	0.189
3.64	0.127	0.144	0.136	0.112

Table 2. Spearman Correlations of metallicity and number of cluster galaxies in a cell

z	Smoothing Radius($^{\circ}$)			
	0	2	3	4
0.187	0.077	0.097	0.078	0.061
0.456	0.084	0.179	0.182	0.167
1.21	0.127	0.274	0.273	0.246
3.64	0.169	0.201	0.189	0.154

tory at different epochs. We use the HEALPix³ algorithm to determine equal area patches on the sky, and calculate the mass weighted average metallicities for each patch and time bin as before. Figure 5 shows the mass-weighted metallicity maps for our four highest redshift bins, smoothed with a boxcar filter of radius 2° . Over-plotted are the locations of the Brightest Cluster Galaxies from the SDSS C4 catalog (Miller et al. 2005), used to represent the distribution of cluster galaxies on the sky. It is clear by eye that in many regions the crosses follow the regions of higher metallicity

For areas of the footprint where cluster galaxies exist, a cross-correlation analysis between mass weighted average gas metallicity and number of cluster members in cells reveals strong correlation between the three oldest bins $z = 0.456, 1.21, 3.64$ and the number of cluster galaxies⁴ (see Tables 1 and 2). It would appear that, as stated in Sheth et al. (2006), metallicity is strongly correlated with environment - this can be interpreted as the seeds of clusters being the seeds of metal enrichment in the universe. Note that the overall level of enrichment in the map at $z = 3.64$ is very homogeneous at around the solar metallicity value, while at $z = 0.187$ there is much more variation. If we assume that metallicity is an indicator of environment, this offers a tantalisingly glimpse of the growth in the influence of dark matter structure, only visible by examining the huge volume at high (temporal rather than spatial) redshift offered by the fossil record.

It will be interesting to cross-correlate these maps with the upcoming SZ experiments which will detect clusters of galaxies at higher redshift. The larger variations in the lowest redshift map probably reflect the change in sampling to less massive galaxies, as these are those in the sample which are likely to have a high fraction of younger star formation.

³ Details of the HEALPix package are available from <http://healpix.jpl.nasa.gov>

⁴ NB: We correlate with cluster members, not BCGs

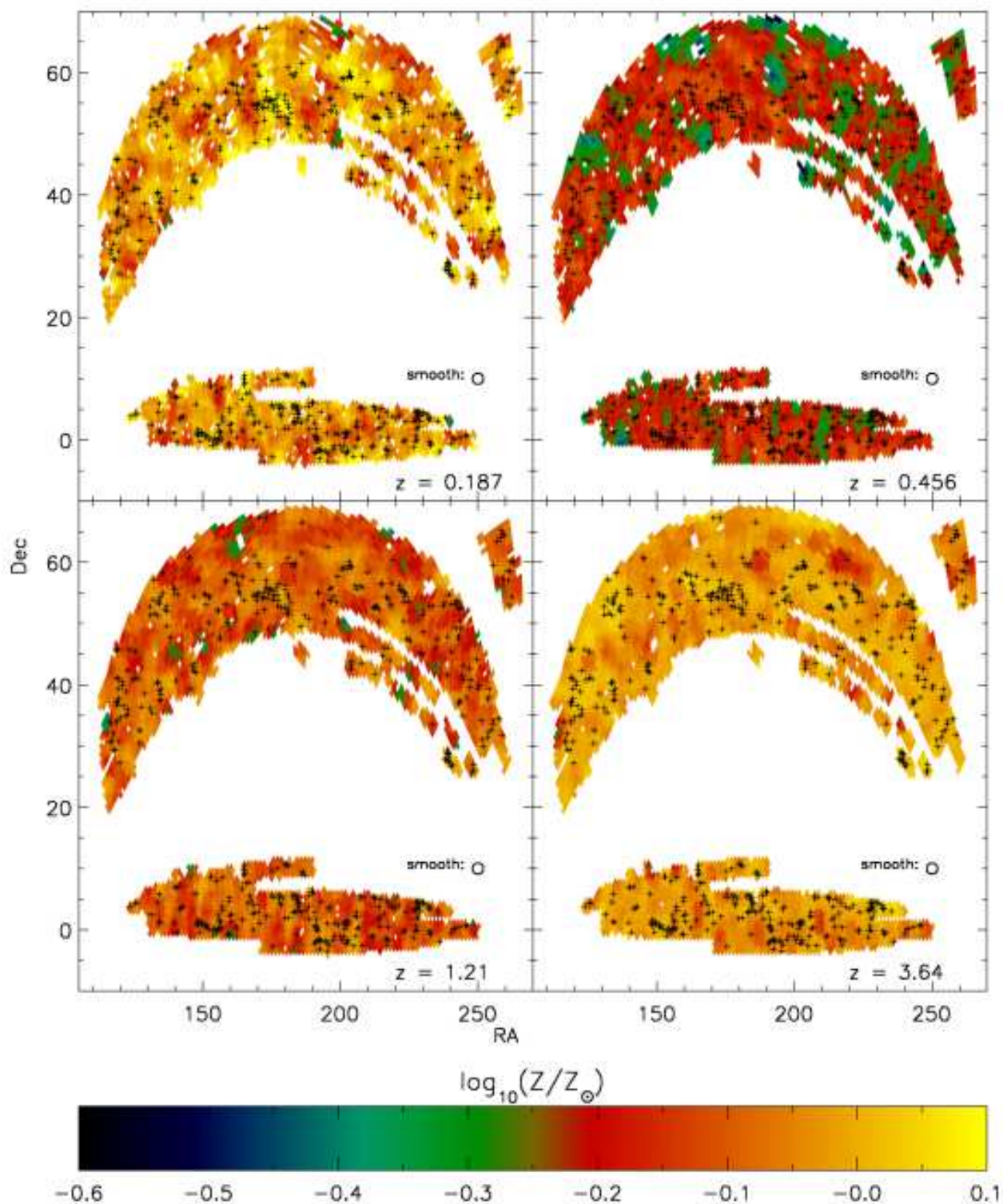


Figure 5. HEALPix projection of the mass weighted gas metallicity for several look back bins averaged over galaxies in the redshift range $0.0 < z < 0.1$. Galaxies only contribute to a bin if $> 25\%$ of their star formation occurs in that bin. The overlaid crosses correspond to the bright cluster members in the C4 catalog. The metallicities are boxcar smoothed over a 2° radius. The size of the smoothing patch is shown in the bottom right of each panel

6 THE AVERAGE MASS-METALLICITY RELATION

We now turn our attention to the local mass-metallicity relation for the SDSS galaxy population to understand its origin and its time evolution.

Fig. 6 shows the mass-metallicity relation for 312,815 galaxies in the DR3 Main Galaxy Sample. In this case we calculate the mass fraction weighted metallicity, ie for an individual galaxy the metallicity is calculated by weighting the bin metallicities by the observed fraction of mass in that bin. The three solid lines represent the 16th, 50th and 84th percentiles of the distribution. The first thing to note is that there is a clear mass-metallicity relation: more massive galaxies harbour stars with higher metallicity. The average metallicity of an L_* galaxy is solar. For lower masses, the metallicity decreases approximately by 0.5dex for every dex in mass.

For galaxies with stellar masses of about $10^9 M_\odot$, the average metallicity of the stars is 0.1 the solar value. Note that for masses larger than $10^{11} M_\odot$ there is a flattening of the mass-metallicity relation. The maximum value we obtain for the mass-metallicity relation is $1.1Z_\odot$. The spread in the relation is also smaller at higher masses (0.15 dex) and grows at smaller masses (0.5 dex).

There is a break around $M_* = 10^{10} M_\odot$, below which the dispersion around the median value increases, and a much wider range of metallicities is recovered for a given mass. This can be interpreted as consistent with the turnover point noted in Kauffmann et al. (2003); Jimenez et al. (2005).

We can obtain a reasonable fit to the median line using a tanh function over the mass range where cells contain more than 2000 galaxies ($8.8 < \log M_* < 11.8$) of the form

$$\log \frac{Z}{Z_\odot} = A + B \tanh \left(\frac{\log M_* - \log M_c}{\Delta} \right) \quad (1)$$

where $\log M_c = 9.66$, $\Delta = 1.04$, $A = -0.452$, $B = 0.572$ and masses are in solar masses. This formula is given purely for convenience, and should not be taken to reflect any underlying physical motivation or be extrapolated outside of the fitted mass range. It is of interest though that the break at $\log M_c = 9.66$ neatly corresponds with the increase in dispersion noted above.

We can now compare this relation with previous work. Recently Gallazzi et al. (2005), using absorption indices in the spectra of SDSS galaxies, have determined the local mass-metallicity relation. Their approach is different from ours since they concentrate on specific absorption features of the spectrum, and their results are weighted towards the most luminous populations. For most old galaxies this will be very similar to our own result, but because we know the contribution to the spectra of each component we can recalculate the average metallicity of galaxies with similar weighting (Fig. 7). The agreement is very good over the matching mass range, although seems to be breaking down at the low-mass end. This is not surprising because due to down-sizing of the galaxy population, it is the low-mass galaxies that dominate star formation today. This of course is due to the fact that for younger galaxies with ongoing star formation it is the younger stars that are more luminous, even though by mass the galaxies are almost certainly dominated by older stars (Panter et al. 2007). The otherwise excellent

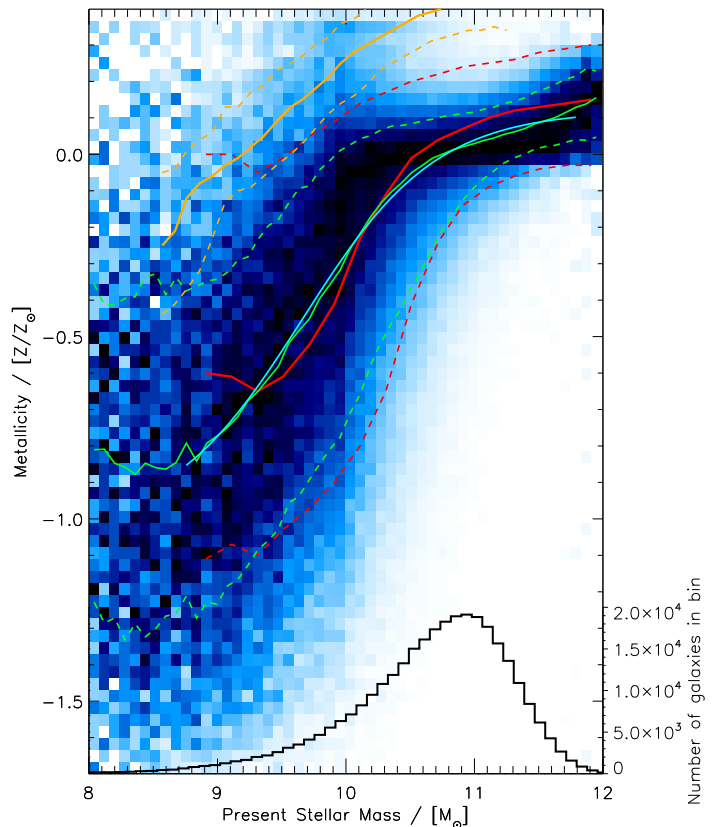


Figure 6. Mean metallicity mass relation using the present mass fractions as weights. The solid green lines represent the 16th, 50th and 84th percentiles of the distribution and the light blue a tanh fit to the results. The dashed and dot-dash lines are the same percentiles for the Gallazzi et al. (2005) (red) and Tremonti et al. (2004) (orange) results. The distributions are normalized over each column of mass, the underlying galaxy mass distribution is shown in the lower histogram

agreement reinforces the fact that we are not introducing degeneracies in the overall quantities by recovering the star and metallicity history in 11 time bins. In Fig. 7 we show the same plot as in Fig. 6 but this time luminosity-weighted (strictly, by spectral flux). Note that in this case there is again good agreement, slightly better than before for lower masses.

We have also overplotted the mass-metallicity relation determined by Tremonti et al. (2004) from emission line measurements, and a clear offset can be seen. In the next section we take advantage of MOPED ability to recover the time evolution of the metallicity and star formation history to explain the difference.

7 RECOVERING THE MASS-METALLICITY RELATION FOR YOUNGER POPULATIONS

Since the MOPED algorithm recovers both the star formation and metallicity history of a galaxy it can be used to investigate the evolution of the metallicity for a given galaxy - a task impossible with simple indices. In particular we can

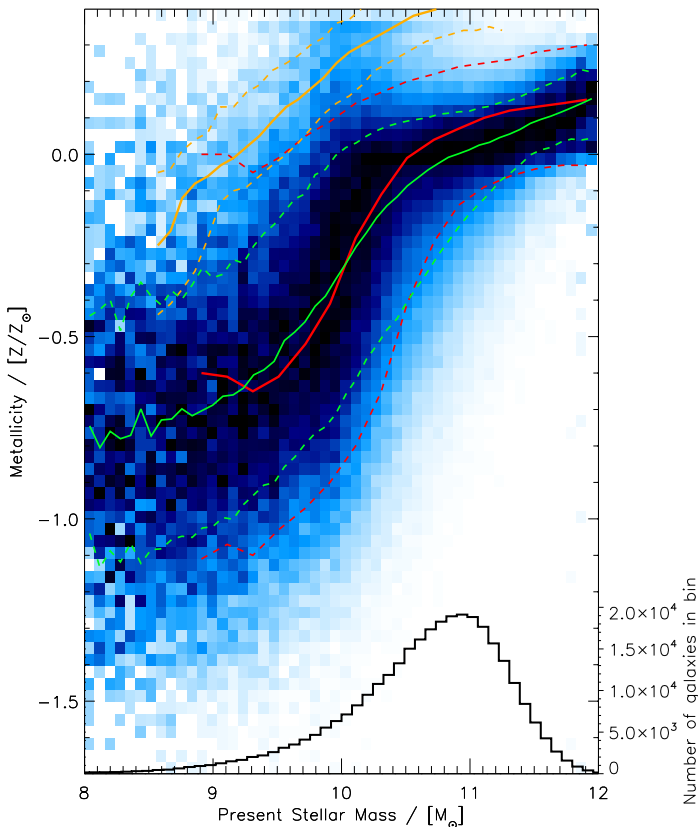


Figure 7. Mean metallicity mass relation using the luminous fractions as weights. The solid line represents the 16th, 50th and 84th percentiles of the distribution. The dashed and dot-dash lines are the same percentiles for the Gallazzi et al. (2005) (red) and Tremonti et al. (2004) (orange) results. The distributions are normalized over each column of mass, the underlying galaxy mass distribution is shown in the lower histogram

look at only galaxies with recent star formation and examine how the metallicity of the star forming gas has evolved from that which produced the majority of the stars at earlier ages.

By using only the younger populations ($\leq 1\text{Gyr}$) of galaxies for the analysis we can reconstruct the information that would be probed by the emission line analysis (as in Tremonti et al. (2004)). Note that our analysis explicitly removes strong emission lines - all our information comes from continuum shape and absorption features. Excluding AGN activity, the emission lines reflect the metallicity of nebular gas around star-forming regions that has been excited by the UV emission of young stars. Fig. 8 shows the mass-metallicity relation of the star-forming gas as derived indirectly from our analysis. It is important to use only metallicities which are well determined - for this analysis we use the 27915 galaxies for which over half the spectral light comes from these younger populations, and plot the metallicity weighted by their fractional spectral flux. Note that now the agreement with the Tremonti et al. (2004) result is much better and our analysis shows that their metallicities are dominated by an intermediate $\sim 1\text{Gyr}$ stellar popula-

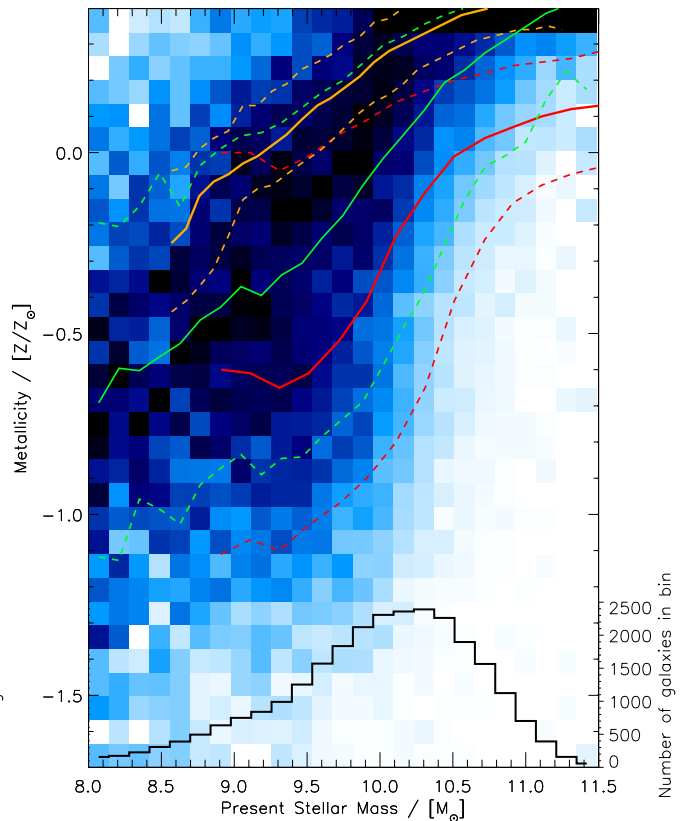


Figure 8. Intermediate-age mass-metallicity relation. To compose this plot we have considered only those galaxies with more than half their spectral flux in populations $\leq 1\text{Gyr}$. The metallicity is the average of the younger bins weighted by their fractional spectral flux. The solid line represents the 16th, 50th and 84th percentiles of the distribution. The dashed and dot-dash lines are the same percentiles for the Gallazzi et al. (2005) (red) and Tremonti et al. (2004) (orange) results. The distributions are normalized over each column of mass, the underlying galaxy mass distribution is shown in the lower histogram

tion in sub- L^* galaxies. In Fig. 9 we extend this analysis by comparing directly the metallicities determined from absorption and emission of galaxies which have more than half of their flux in populations $\leq 1\text{Gyr}$. The figure shows good agreement, confirming that given sufficient flux in those populations the MOPED algorithm using absorption features can determine accurate metallicities. The offset could indicate a systematic difference in metallicity between the birth cloud (responsible for the emission features) and the young stars, or possibly a calibration offset in the models.

We can extend this analysis to galaxies younger than the 1 Gyr bin, although the number of galaxies with sufficient star formation in these youngest age bins is very small and determination of metallicity in these younger stars with weaker absorption features is more difficult than in older, cooler stars. Fig. 10 shows the mass-metallicity relation of these younger populations and it is clear that any relationship has broken down. First, the stellar mass range is much smaller than before because of downsizing in the galaxy population. Only galaxies with stellar masses below 10^{10}

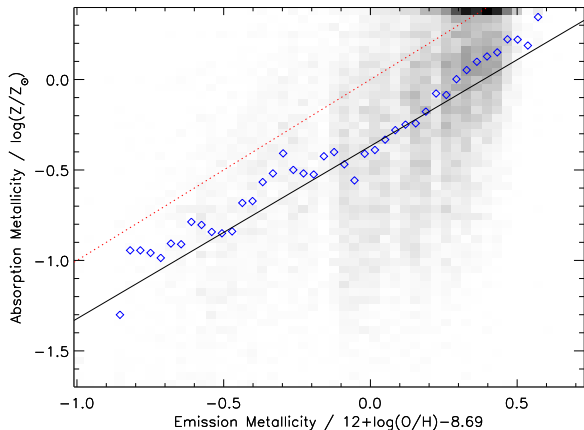


Figure 9. A comparison of metallicities determined by absorption and emission analysis. This plot considers only those 14038 galaxies with more than half their spectral flux in populations ≤ 1 Gyr that also have a metallicity reported in the Tremonti et al. (2004) sample. The absorption metallicity is the average of the younger bins weighted by their fractional spectral flux and the emission metallicity is taken from Tremonti et al. (2004). The blue diamonds show the median value of absorption metallicity for a given emission metallicity, the black line is a linear fit through all points and the red dotted line corresponds to a 1:1 relation. See text for a discussion of the offset.

M_{\odot} contribute significantly to the young population metallicity and the mass range is only of 1.5 dex. As pointed out earlier the mass-metallicity relation is flat (at least for $M < 10^{10.5} M_{\odot}$), with no dependence on mass and an average metallicity of $0.2Z/Z_{\odot}$. Why galaxies below this mass all have the same metallicity is something we will investigate in future work, but one could envision environment as a major driver, where the gas in filaments that feed the galaxy has been enriched to a certain level.

8 MODEL DEPENDENCE OF THE METALLICITY HISTORY

The results shown so far have all been generated using the current standard in stellar modelling codes, Bruzual & Charlot (2003). It is important however to consider the effect of changing the models used; we make no statement as to which set is “right”, and emphasize that the set of galaxies chosen for comparison, detailed in Panter et al. (2007), is relatively small (808).

We have investigated the impact of model choices by recovering the metallicity history with a suite of different stellar population models: SPEED (Jimenez et al. 2004), PEGASE (Fioc & Rocca-Volmerange 1997), BC93 (Bruzual & Charlot 1993), Maraston (Maraston 2005), GALAXEV (Bruzual & Charlot 2003), CB07 (As BC03 but an with improved treatment of TP-AGB stars). Our reference model is the BC03 at a spectral resolution of 3\AA .

In Fig. 11 we show the differences in average metallicity of stars as a function of redshift. It is clear that our conclusions regarding higher-mass galaxies having higher metallicity is robust whichever model is used. The deviation shown by the SPEED models reflects the fact that, as shown in Panter et al. (2007), the star formation history recovered by

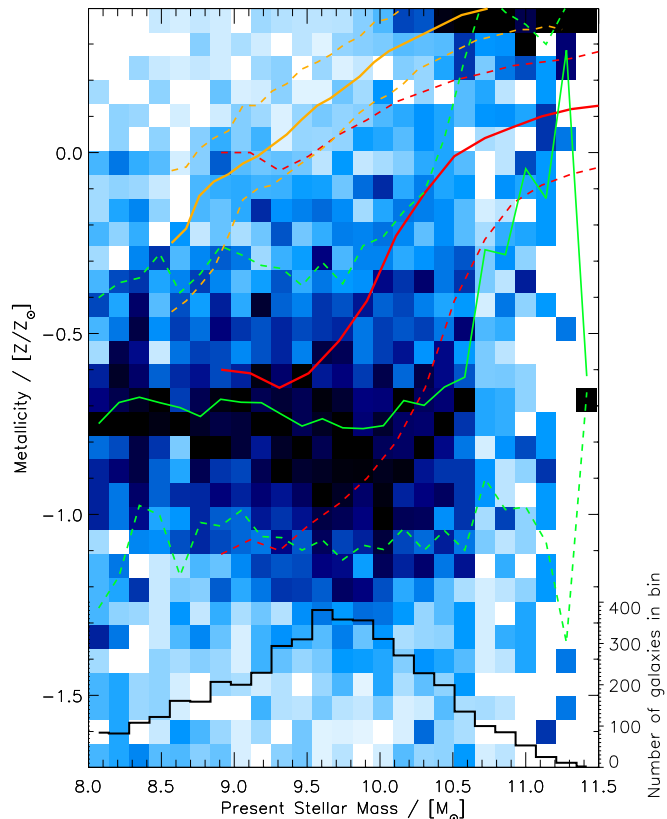


Figure 10. Youngest age mass-metallicity relation. To compose these plots we have considered only those galaxies with more than half their spectral light in populations < 1 Gyr. The metallicity is the average of the younger bins weighted by their fractional spectral flux. The solid line represents the 16th, 50th and 84th percentiles of the distribution. The dashed and dot-dash lines are the same percentiles for the Gallazzi et al. (2005) (red) and Tremonti et al. (2004) (orange) results. The distributions are normalized over each column of mass, the underlying galaxy mass distribution is shown in the lower histogram

this model is broader, with overall SFR peaking at $z < 1$. It should also be noted that the SPEED models allow a wider range of metallicity values than other synthesis codes.

In Fig. 12, there is apparently some issue at $z=0.2$ ($t \sim 1$ Gyr), where almost all the models give very similar metallicity. With a population of galaxies taken at $z = 0.1$, this corresponds to a population of stars of age 1 Gyr, in some respects a difficult population to identify as no part of the spectrum is dominated by this population for usual star formation histories (Panter et al. 2007; Mathis et al. 2006). As this age reflects the point for the average galaxy where flux per population is at a minimum, we caution against over-interpretation. Although it may be a systematic failing of the libraries used to calibrate the various sets of models it seems more likely that what is being reflected is the prior introduced by a fiducial metallicity. Alternatively, it could be that a more sophisticated treatment of the post-AGB stages, as included in the more modern models, removes the problem. Whichever set of models is chosen, the redshift

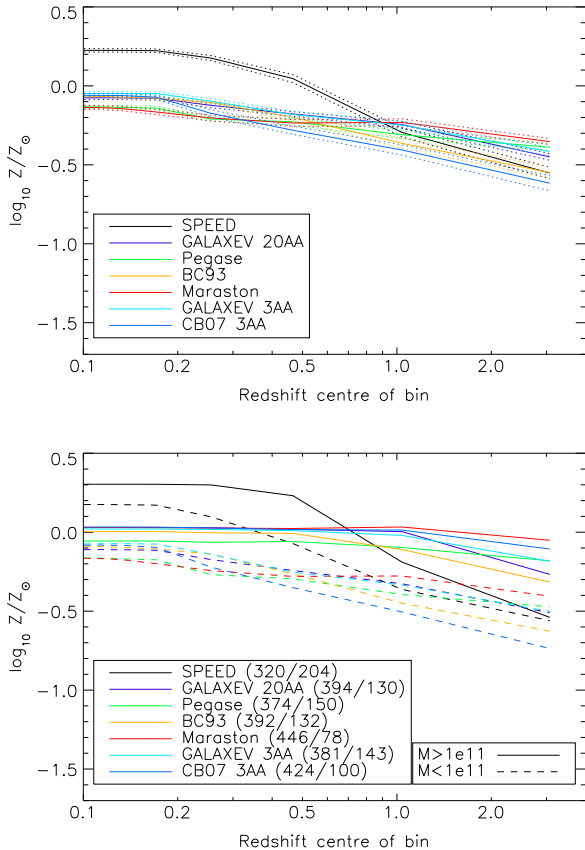


Figure 11. Cumulative metallicity of stars in SDSS galaxies recovered using different stellar population models. The lower panel illustrates the difference between low and high mass galaxies.

evolution of the stellar metallicity in the SDSS population is fairly flat, with a variation of about 0.5 dex.

Of particular interest are the differences between the Maraston, SPEED and CB07 models. These three each include a treatment of mass loss along the thermal-pulsating AGB phase of stellar evolution. The SPEED models incorporate this effect using an empirical prescription (Jorgensen 1991; Jimenez et al. 1998; Jimenez et al. 2004). If we focus on these models which include mass loss (Maraston, SPEED and CB07) then the discrepancy in recovery of metallicity is of about 0.1 dex beyond $z=1$, but diverges by 0.5 dex at lower redshifts. Clearly the metallicity is more sensitive to the model choice than the star formation history (see Panter et al. (2007)) and the error budget in determining the metallicity history is dominated by the choice of model. Further work is needed to calibrate the models with higher accuracy.

Figure 13 shows in different panels the effect of various systematics. It is clear from Fig. 13(a) that changing the photometric reduction pipeline will have an effect on the metallicity values recovered (the SPEED model was used for this comparison, GALAXEV for the following). The changes from DR1 to DR3 are clear, but it appears that PCA skyline (Wild & Hewett 2005) cleaning does nothing to change the recovered metallicity history. Fig. 13(b) makes it clear that, for a model calculated and calibrated at 3Å but rebinned to

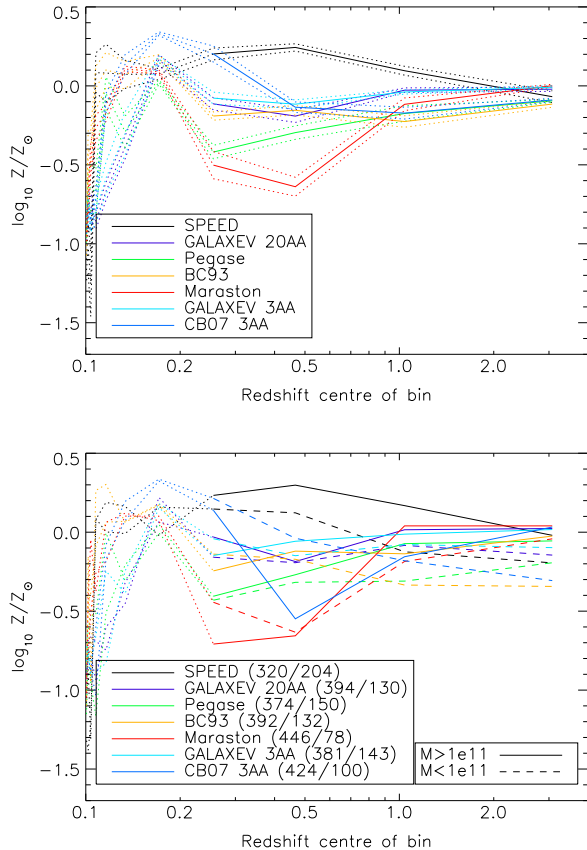


Figure 12. Metallicity of star forming gas in SDSS galaxies recovered using different stellar population models. We caution that the region lower than $z = 0.3$ (dotted) has relatively little flux, and is not used for our earlier analysis.

20Å it is still possible to recover the same metallicity history. It is interesting however to note that this is the only change which has any effect on the 1 Gyr bump evident in most of other stellar population models, but further analysis is required (with many more galaxies and rebinning resolutions) to resolve this issue. Figures 13(c) and 13(d) show that changing IMF and dust extinction curve do not alter the metallicities recovered by a large amount. The apparently large variations in the right hand panels can be explained by the changes in galaxy mass, caused by changing either the IMF or extinction curve, moving galaxies between the two samples.

9 CONCLUSIONS

In this paper we have presented the cosmic evolution of the bulk metallicity of galaxies, demonstrating a clear trend of downsizing which is robust to the selection of stellar population model to determine the metallicity of the galaxy. We have extended this to explore the evolution of metallicity of star forming gas, which also follows a downsizing scenario but is more dependent on the choice of stellar model. The trend shows how massive galaxies have higher metallicities at earlier times while less massive galaxies have lower

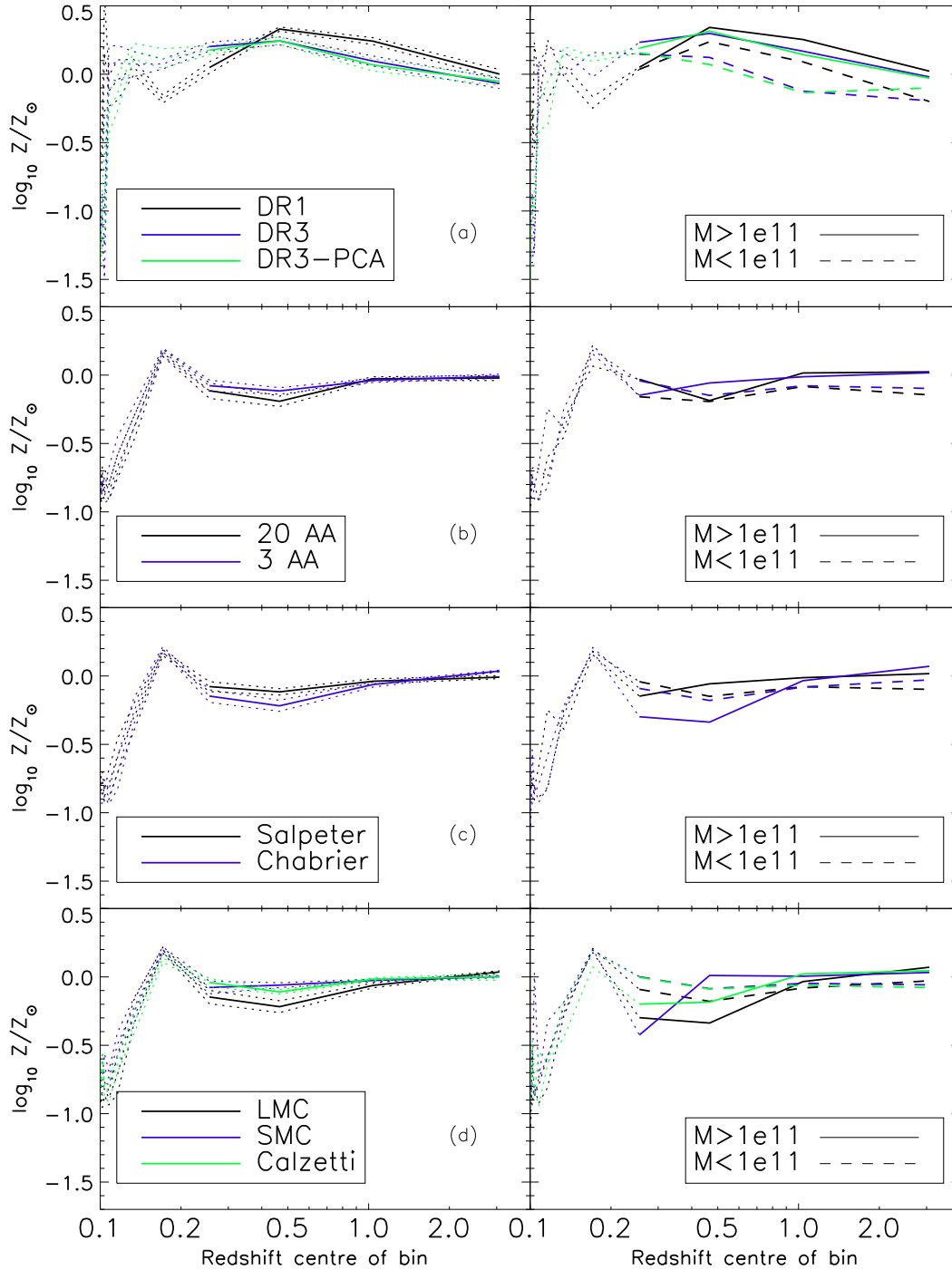


Figure 13. Effect of several systematic effects on the determination of the metallicity from the spectra of the stellar populations of galaxies (left), and how they effect conclusions based on mass (right). The different panels show the effect of different systematics: Fig. (a) shows the effect of different pipelines in the data reduction of the SDSS spectra, the error is comparable to the random error, although it is clear that there is a difference between the DR1 and DR3 reductions. Fig. (b) shows the effect of spectral resolution in the models; it would not be surprising to see a difference when the spectral resolution is increased, but this is not evident. This could be due to the fact that the underlying model (BC03) is calibrated at 3\AA and rebinned to 20\AA . Fig. (c) shows the difference by choice of IMF - the overall change in recovered metallicity of the star forming gas is small, but the large changes in mass around the cut (due to the strong dependence of mass on the IMF) give a misleading effect on the right hand plot. Fig. (d) shows the dependence on dust model choice, and again the variation on the right hand figure is due to mass differences rather than a large difference in recovered metallicity.

metallicities at earlier times but reach the same metallicity at about 1 Gyr from the current time. We have shown a clear correlation between metallicity and cluster environment, and will perform more correlations as further datasets become available.

We have reconciled the disparity between the mass-metallicity relations recovered from nebular emission line spectra and stellar absorption methods. As one might expect, the absorption method is entirely appropriate for estimating the metallicity of older, established galaxies, while it may fail for galaxies which are undergoing recent star formation where the most luminous population is almost certainly not the most massive in stellar mass. We have verified that the fossil analysis technique, which here excludes emission lines, can be used simultaneously to uncover the metallicities of both young and old populations by producing a mass-metallicity relation that accurately maps the results given by both emission and absorption line diagnostics.

It is clear from the comparison of stellar models that the metallicity history determined for the star forming gas is highly model dependent. Although we use models with a wide range of publication dates, it is apparent that the three most modern show the largest deviation. We acknowledge that alpha enhancement, not included in any of the stellar population models we consider, could affect the metallicities we recover.

ACKNOWLEDGMENTS

A portion of BDP's work was supported by the Alexander von Humboldt Foundation, the Federal Ministry of Education and Research, and the Programme for Investment in the Future (ZIP) of the German Government. We acknowledge the use of HEALPix (Górski et al. 2005) and software packages developed by David Fanning (Fanning Consulting), and the assistance of Gerard Lemson and GAVO for access to the Millennium/SDSS Database and advice on SQL. We thank Manuchehr Taghizadeh-Popp for assistance in the identification of SDSS galaxies in the Healpix tessellation scheme. Funding for the SDSS has been provided by the Alfred P. Sloan Foundation, the Participating Institutions, the National Science Foundation, the U.S. Department of Energy, NASA, the Japanese Monbukagakusho, and the Max Planck Society. RJ is supported by grants from the Spanish Ministry of Science (MEC), the Spanish Higher Council for Scientific Research (CSIC) and the European Union (IRG).

REFERENCES

- Abazajian, K., et al. (the SDSS collaboration) 2005, *AJ*, 129, 1755
- Bouché N., Lehnert M. D., Aguirre A., Péroux C., Bergeron J., 2007, *MNRAS*, 378, 525
- Bruzual A. G., Charlot S., 1993, *ApJ*, 405, 538
- Bruzual G., Charlot S., 2003, *MNRAS*, 344, 1000
- Cid Fernandes, R., Mateus, A., Sodré, L., Stasińska, G., & Gomes, J. M. 2005, *MNRAS*, 358, 363
- Cid Fernandes R., Asari N. V., Sodré L., Stasińska G., Mateus A., Torres-Papaqui J. P., Schoenell W., 2007, *MNRAS*, 375, L16
- Erb D. K., 2008, *ApJ*, 674, 151
- Erb D. K., Shapley A. E., Pettini M., Steidel C. C., Reddy N. A., Adelberger K. L., 2006, *ApJ*, 644, 813
- Fioc M., Rocca-Volmerange B., 1997, *A&A*, 326, 950
- Freeman K., Bland-Hawthorn J., 2002, *ARA&A*, 40, 487
- Gallart, C., Zoccali, M., & Aparicio, A. 2005, *AR&A*, 43, 387
- Gallazzi, A., Charlot, S., Brinchmann, J., White, S. D. M., & Tremonti, C. A. 2005, *MNRAS*, 362, 41
- Gallazzi, A., Charlot, S., Brinchmann, J., & White, S. D. M. 2006, *MNRAS*, 370, 1106
- Gallazzi A., Brinchmann J., Charlot S., White S. D. M., 2008, *MNRAS*, 383, 1439
- Gordon, K. D., Clayton, G. C., Misselt, K. A., Landolt, A. U., Wolff, M. J., 2003, *ApJ*, 594, 279
- Górski, K. M., Hivon, E., Banday, A. J., Wandelt, B. D., Hansen, F. K., Reinecke, M., & Bartelmann, M. 2005, *ApJ*, 622, 759
- Heavens, A. F., Jimenez, R., & Lahav, O. 2000, *MNRAS*, 317, 965
- Heavens, A., Panter, B., Jimenez, R., & Dunlop, J. 2004, *Nature*, 428, 625
- Jimenez, R., Padoan, P., Matteucci, F., & Heavens, A. F. 1998, *MNRAS*, 299, 123
- Jimenez R., MacDonald J., Dunlop J. S., Padoan P., Peacock J. A., 2004, *MNRAS*, 349, 240
- Jimenez, R., Panter, B., Heavens, A. F., & Verde, L. 2005, *MNRAS*, 356, 495
- Jorgensen, U. G. 1991, *A&A*, 246, 118
- Kauffmann, G. et al. 2003, *MNRAS*, 341, 33
- Kewley, L. J., & Dopita, M. A. 2002, *ApJS*, 142, 35
- Maiolino, R., et al., astro-ph, arXiv.org:0712.2880
- Maraston C., 2005, *MNRAS*, 362, 799
- Mateus, A., Sodre, L., Cid Fernandes, R., & Stasińska, G. 2006, *MNRAS*, submitted (astro-ph/0604063)
- Mathis, H., Charlot, S., & Brinchmann, J., 2006, *MNRAS*, 365, 385
- Miller, C. J., et al. 2005, *AJ*, 130, 968
- Ocvirk, P., Pichon, C., Lançon, A., & Thiébaud, E., 2006, *MNRAS*, 365, 46
- Panter, B., Heavens, A. F., & Jimenez, R. 2003, *MNRAS*, 343, 1145
- Panter, B., Heavens, A. F., & Jimenez, R. 2004, *MNRAS*, 355, 764
- Panter, B., Jimenez, R., Heavens, A. F., & Charlot, S. 2007, *MNRAS*, 378, 1550
- Pettini, M. 2001, *The Promise of the Herschel Space Observatory*, 460, 113
- Reichardt, C., Jimenez, R., & Heavens, A. F. 2001, *MNRAS*, 327, 849
- Sheth, R. K., Jimenez, R., Panter, B., & Heavens, A. F. 2006, *ApJL*, 650, L25
- Tojeiro, R., Heavens, A. F., Jimenez, R., & Panter, B. 2007, *MNRAS*, 381, 1252
- Tremonti C. A. et al., 2004, *ApJ*, 613, 898
- Wild V., Hewett P. C., 2005, *MNRAS*, 358, 1083
- Worthey, G. 1994, *ApJS*, 95, 107